Extreme Sensitivity of a Topochemical Reaction to Cation Substitution: $SrVO_2H$ vs $SrV_{1-x}Ti_xO_{1.5}H_{1.5}$.

Midori Amano Patino [†], Dihao Zeng [†], Stephen J. Blundell [‡], John E. McGrady [†] and Michael A. Hayward [†]*.

[†] Department of Chemistry, University of Oxford, Inorganic Chemistry Laboratory, South Parks Road, Oxford, OX1 3QR, United Kingdom.

[‡] Department of Physics, Clarendon Laboratory, University of Oxford, Parks Road, Oxford, OX1 3PU, UK.

Supporting Information Placeholder

ABSTRACT: The anion-ordered oxide-hydride $SrVO_2H$ is an antiferromagnetic insulator due to strong correlations between vanadium d-electrons. In an attempt to hole-dope $SrVO_2H$ into a metallic state, a strategy of first preparing $SrV_{1-x}Ti_xO_3$ phases and then converting them to the corresponding $SrV_{1-x}Ti_xO_2H$ phases *via* reaction with CaH_2 was followed. This revealed that the solid-solution between $SrVO_3$ and $SrTiO_3$ is only stable at high temperature. In addition reactions between $SrV_{0.95}Ti_{0.05}O_3$ and CaH_2 were observed to yield $SrV_{0.95}Ti_{0.05}O_{1.5}H_{1.5}$ not $SrV_{0.95}Ti_{0.05}O_2H$. This dramatic change in reactivity for a very modest change in initial chemical composition is attributed to an electronic destabilization of $SrVO_2H$ on titanium substitution. DFT calculations indicate that the presence of an anion-ordered, tetragonal $SrMO_2H$ phase is uniquely associated with a d^2 electron count, and that titanium substitution leads to an electronic destabilization of $SrV_{1-x}Ti_xO_2H$ phases which, ultimately, drives further reaction of $SrV_{1-x}Ti_xO_2H$ to $SrV_{1-x}Ti_xO_{1.5}H_{1.5}$. The observed sensitivity of the reaction products to the chemical composition of initial phases highlights some of the difficulties associated with electronically doping metastable materials prepared by topochemical reactions.

Introduction

Low-temperature, structure-conserving reactions can be used to manipulate the anion lattices of complex transition-metal oxides, offering routes to highly metastable phases which cannot be readily prepared via conventional high-temperature synthesis. 'Topochemical' reactions of this type have been used to generate extended solids containing arrays of transition-metal cations in highly unusual oxidation-state/coordination-geometry combinations.[1-3] For example, by utilising binary metal hydrides such as NaH, LiH or CaH_2 as reducing agents,[4] it has proved possible to deintercalate oxide ions from transition-metal oxide perovskites to yield phases containing square-planar Fe^{2+}, Co^{1+}, Ni^{1+} or Ru^{2+} cations.[5-8] In addition hydride-for-oxide anion exchange reactions can also occur, leading to the formation of transition-metal oxide-hydride phases such as $LaSrCoO_3H_{0.7}$, $Sr_3Co_2O_{4.33}H_{0.84}$, $A^{II}TiO_{3-x}H_y$ and the $Sr_{n+1}V_nO_{2n+1}H_n$ series,[9-12] all of which contain reduced transition-metal cations in oxide-hydride coordination spheres. The very unusual electronic structures of these metastable solid-state compounds mean that they are of intrinsic chemical interest, but their electronic and magnetic properties, which arise from the cooperative interactions between the paramagnetic centers, also offer the potential for novel materials properties. Unfortunately, the majority of the reported anion-vacancy ordered reduced oxides and oxide-hydrides prove to be antiferromagnetic insulators, simply because large on-site electron-electron repulsion terms (U) tend to localize the unpaired metal d-electrons on discrete metal cation sites. Valence-electron localization of this type is frequently observed in transition metal oxide phases – even those prepared *via* high-temperature routes – and is particularly common in systems containing 3d transition metal cations in integer oxidation states.[13] Itinerant electrons can, however, be generated *via* chemical 'doping', which drives the transition-metal ions into non-integer or mixed valent states. A classic example is the Cu^{2+} phase La_2CuO_4 which is a simple antiferromagnetic insulator in its pure form. However, doping the system, *via* barium-for-lanthanum substitution leads to a mixed valent $Cu^{2+/3+}$ state which exhibits both metallic conductivity and superconductivity.[14] Likewise the Mn^{3+} and Mn^{4+} phases, $LaMnO_3$ and $CaMnO_3$, are both antiferromagnetic insulators,[15-16] but mixed valent $Mn^{3+/4+}$ members of the $La_{1-x}Ca_xMnO_3$ solid solution exhibit metal-insulator transitions and large magnetoresistive ratios.[17]

The remarkable differences in physical properties of the doped and undoped oxides provide strong motivation to explore the effects of doping on topochemically prepared phases. The oxide-hydride $SrVO_2H$ is an ideal candidate in this respect.[12] As shown in Figure 1, $SrVO_2H$ adopts an anion-ordered structure in which the V^{3+} cations reside within *trans*-VO_4H_2 local coordination sites which then share corners to form a 3D network. The ordered arrangement of oxide and hydride anions lifts the degeneracy of the π-symmetry vanadium d-orbitals (d_{xz}, d_{yz}, d_{xy}), giving a local $(d_{xz/yz})^2(d_{xy})^0(d_{z^2})^0(d_{x^2-y^2})^0$ configuration. Substantial on-site repulsions split the half-filled $d_{xz/yz}$ band, leading to a Mott-Hubbard insulating state.[12, 18-19] In very recent work we have demonstrated that $SrVO_2H$ undergoes a pressure induced insulator-to-metal transition at ~50 GPa.[20] The resulting metallic state exhibits a significant 2-dimensional character because the hydride ions block dispersion along the z-axis of the π-symmetry bands which span the Fermi level. A detailed study of this pressure-induced metallic state is, unfortunately, experimentally very challenging and so we hope to gain an alternative perspective on this material *via* hole-doping with Ti, which should partially depopulate the $d_{xz/yz}$ band and hence generate a metallic state at ambient pressure. Here we describe our attempts to hole-dope $SrVO_2H$, first by preparing samples of titanium-substituted $SrV_{1-x}Ti_xO_3$, and then reducing them to form oxide-hydride phases. In the course of these studies we observed that the low-temperature anion-exchange reaction which forms the oxide-hydride phases is

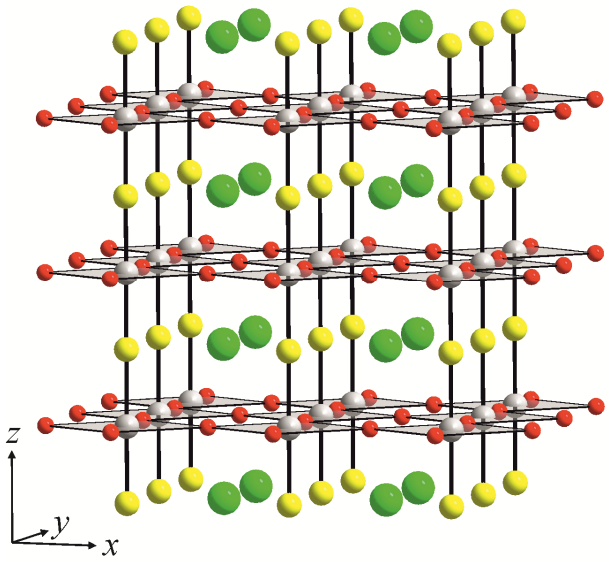

Figure 1 The crystal structure of $SrVO_2H$. Green, grey, red and yellow spheres represent Sr, V, O and H respectively.

extremely sensitive to even very small changes in the composition of the 'parent' oxide. The Ti-doped analogue of $SrVO_2H$, $SrV_{1-x}Ti_xO_2H$, is only transiently stable, reacting further to form $SrV_{1-x}Ti_xO_{1.5}H_{1.5}$, the doped analogue of the inaccessible $SrVO_{1.5}H_{1.5}$ phase. This extreme sensitivity to chemical substitution has important implications for doping strategies of other topochemically prepared materials.

Experimental

Synthesis of $SrV_{1-x}Ti_xO_3$. The synthesis of $SrV_{1-x}Ti_xO_3$ samples was attempted in two different ways, a 'ceramic' synthesis route and an 'arc-melt' route. The ceramic synthesis of $SrV_{1-x}Ti_xO_3$ utilized a modified version of the procedure previously described to prepare $SrVO_3$.[21] Suitable ratios of $SrCO_3$ (99.99%), V_2O_5 (99.99%) and TiO_2 (99.995%, previously dried at 900 °C) were ground together and then heated in air at 900 °C for 12 h to decompose the carbonate and prepare $Sr_2V_{2-2x}Ti_{2x}O_{7-\delta}$, as confirmed by powder X-ray diffraction. Samples were then heated at 1075 °C, under flowing H_2 (100%), for multiple periods of 12 h with intermediate grinding, until no further changes were observed in X-ray powder diffraction patterns. $SrV_{1-x}Ti_xO_3$ samples were also prepared *via* arc-melting. Suitable stoichiometric ratios of SrO (prepared by heating $SrCO_3$ under vacuum at 1100 °C), V_2O_3 (99.7%), and TiO_2 were thoroughly mixed inside an argon filled glovebox, pressed into pellets and transferred to the arc-melt furnace without being exposed to air. The furnace was purged with argon and the pellets were melted a total of four times in an electrical discharge arc, on a water-cooled copper hearth, with each pellet being turned between heatings. Samples were allowed to cool for 15 minutes inside the furnace under flowing argon before immediately being transferred to an argon filled glovebox.

Reduction of $SrV_{1-x}Ti_xO_3$. Samples of $SrV_{1-x}Ti_xO_3$ were reacted with CaH_2 as described previously for the synthesis of $SrVO_2H$ from $SrVO_3$.[12] Powder samples of $SrV_{1-x}Ti_xO_3$ were ground together with 2 mole equivalents of CaH_2 in an argon-filled glove box and then sealed under vacuum in amorphous-silica ampoules. Samples were then heated at 610 °C for multiple 2 day periods (as described in the text below) with regrinding between heating periods. Reaction products were washed, under an inert atmosphere, with 4 x 100 ml of a 0.1 M solution of NH_4Cl in methanol, followed by 4 x 100 ml of clean methanol in order to remove unreacted CaH_2 and reaction by-products (CaO).

Characterization. X-ray powder diffraction data were collected from samples sealed under argon in gas-tight sample holders using a PANalytical X'Pert diffractometer incorporating an X'celerator position sensitive detector (monochromatic Cu $K_{\alpha 1}$ radiation). High-resolution synchrotron X-ray powder diffraction data were collected using instrument I11 at the Diamond Light Source Ltd. Diffraction patterns were collected using Si-calibrated X-rays with an approximate wavelength 0.825 Å, from samples sealed in 0.5mm diameter borosilicate glass capillaries. All samples were diluted with an equal volume of amorphous boron to limit absorption. Rietveld profile refinements were performed using the GSAS suite of programs.[22] Magnetization data were collected using a Quantum Design MPMS SQUID magnetometer. The μ^+SR experiments were carried out using the GPS instrument at the Swiss Muon Source, PSI, Switzerland. In a μ^+SR experiment, spin-polarized muons were implanted in the bulk of a material and the time-dependence of their polarization monitored by recording the angular distribution of the subsequent positron decay. Thermogravimetric measurements were performed by heating powder samples at a rate of 5 °C·min^{-1} under an oxygen atmosphere, using a Mettler-Toledo MX1 thermogravimetric microbalance. Manganometric titrations were performed by dissolving samples in 5M H_2SO_4 and then titrating the resulting solution against $KMnO_4$.

DFT calculations. All density functional calculations were performed using the VASP software package (VASP 5.3),[23] with the PBE density functional[24] and an effective Hubbard U (U_{eff}) of 2.0 eV on Ti and V centers was used to describe the effect of strong correlations. A plane-wave cutoff of 600 eV was imposed in all cases and the Brillouin zone was sampled on an 8 × 8 × 7 Γ-centered grid. In order to investigate different models of anion disorder in $SrTiO_2H$, we consider a $\sqrt{2} \times \sqrt{2} \times 2$ expansion of the primitive unit cell which contains four transition metal centers (Figure 6). All the configurations were modelled as G-type antiferromagnets. Geometry optimizations were performed with the unit cell volume constraint released and all ions allowed to relax.

Results

$SrVO_3$-$SrTiO_3$ solubility. X-ray powder diffraction data collected from $SrV_{1-x}Ti_xO_3$ (x = 0.05, 0.4, 0.5) samples prepared by the ceramic route (Figures 2 and S1) could be indexed on the basis of two primitive cubic phases with lattice parameters in close agreement to the reported parameters of $SrVO_3$ (3.840 Å)[21] and $SrTiO_3$ (3.905 Å)[25]. Thus 2-phase models based on the structures of $SrVO_3$ and $SrTiO_3$ were refined against the data to yield lattice parameters and phase fractions listed in Table 1 (top). The very close correspondence between the lattice parameters of the two phases with those of $SrVO_3$ and $SrTiO_3$, combined with correspondence between the fraction of phase 2 ($SrTiO_3$) and the Ti content of the original mixture, suggests that there is almost no solubility between $SrVO_3$ and $SrTiO_3$ under these 'ceramic' synthesis conditions.

X-ray powder diffraction data collected from $SrV_{1-x}Ti_xO_3$ samples prepared by the arc-melt route are shown in Figures 2 and S1. Two primitive cubic phases are again required to model the data, but the refined lattice parameters (listed in Table 1) do not correspond to either $SrVO_3$ or $SrTiO_3$. Moreover, unlike the phases generated by ceramic synthesis, the refined lattice parameters are dependent on sample composition. Finally, the fractions of the two phases do not correlate with the Ti content of the samples as closely as those from the ceramic route. This accumulated evidence indicates that while perfect, single-phased solid-solutions were not prepared *via* the arc-melt route, there is some solubility between $SrVO_3$ and $SrTiO_3$ under the arc-melt conditions and that the sample of nominal composition $SrV_{0.95}Ti_{0.05}O_3$ (*i.e.* that formed from 5% Ti content in the starting material) does contain

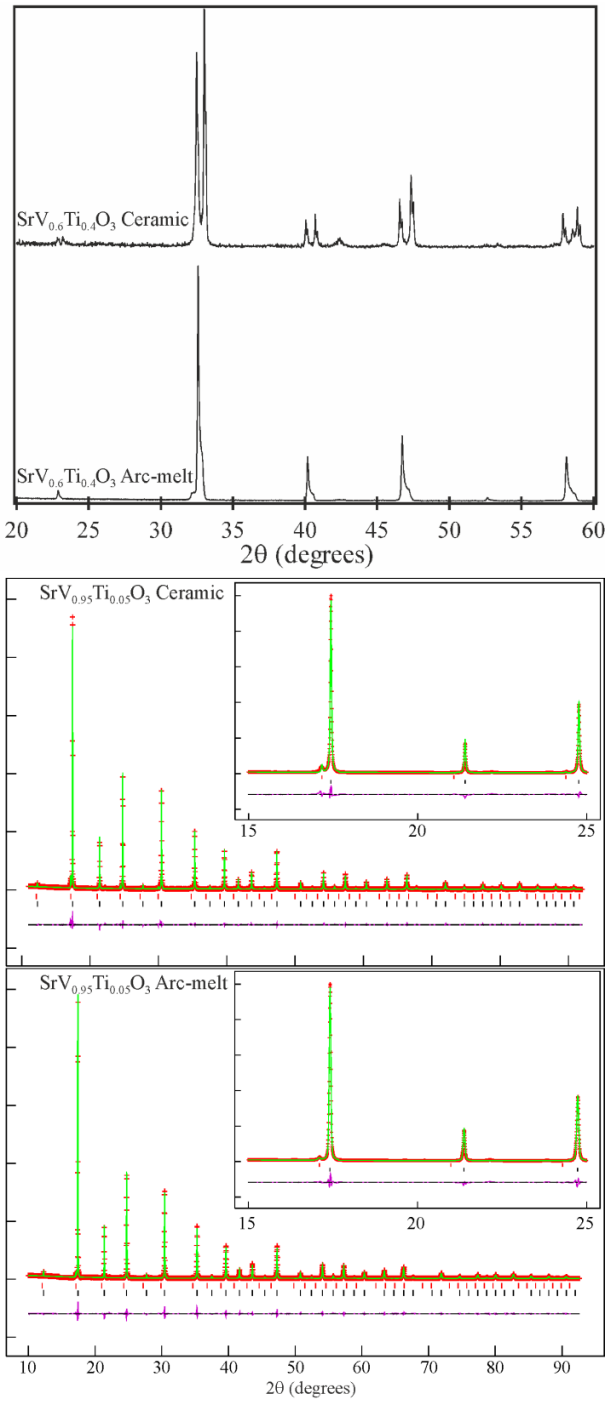

Figure 2. (top) X-ray powder diffraction data collected from samples of nominal composition $SrV_{0.6}Ti_{0.4}O_3$ prepared by ceramic and arc-melt routes. (bottom) Observed, calculated and difference plots from the 2-phase refinements against synchrotron X-ray powder diffraction data of samples of nominal composition $SrV_{0.95}Ti_{0.05}O_3$ prepared by ceramic and arc-melt routes.

some titanium dissolved in the majority phase. For the sake of simplicity, this majority phase will henceforth be referred to as '$SrV_{0.95}Ti_{0.05}O_3$', although the titanium content is lower than this formula indicates. To investigate the stability of these $SrV_{1-x}Ti_xO_3$ solid-solutions, 2 aliquots of the arc-melt prepared $SrV_{0.95}Ti_{0.05}O_3$ sample were sealed in evacuated amorphous-silica ampoules and then heated, one at 600 °C and the other at 1100 °C, for 7 days

Ceramic Samples				
	Phase 1		Phase 2	
Ti content (%)	*a* (Å)	fraction (%)	*a* (Å)	fraction (%)
5	3.8471(1)	95.5(3)	3.9063(1)	4.5(3)
40	3.8439(2)	57.2(5)	3.9041(2)	42.8(5)
50	3.8463(1)	48.3(4)	3.9035(1)	51.7(4)
Arc-melt Samples				
	Phase 1		Phase 2	
Ti content (%)	*a* (Å)	fraction (%)	*a* (Å)	fraction (%)
5	3.8513(1)	97.3(1)	3.9214(1)	2.7(1)
40	3.8610(1)	38.1(3)	3.8832(1)	61.9(3)
50	3.8742(1)	37.9(4)	3.8900(1)	62.1(4)
5 (annealed 600 °C)	3.8510(1)	97.2(1)	3.9210(1)	2.8(1)
5 (annealed 1100 °C)	3.8432(1)	94.7(2)	3.9020(1)	5.3(2)

Table 1. Lattice parameters and phase fractions from the structural refinement of $SrV_{1-x}Ti_xO_3$ samples prepared by ceramic and arc-melt routes.

and then cooled at 2 °C·min^{-1} to ambient temperature. Refinement of the X-ray powder diffraction data from the annealed samples shows that the solid solution is stable at 600 °C but not at 1100°C, where it reverts to a mixture of $SrVO_3$ and $SrTiO_3$ (as indicated by the parameters in Table 1). Manganometric titrations of the ceramic and arc-melted samples of $SrV_{0.95}Ti_{0.05}O_3$ indicated both samples had average vanadium oxidation states of V +3.99(2) and V +4.00(2) respectively and were thus oxygen stoichiometric, as described in detail in the Supporting Information.

Topochemical reduction of '$SrV_{0.95}Ti_{0.05}O_3$'. Samples of '$SrV_{0.95}Ti_{0.05}O_3$' prepared *via* both ceramic and arc-melt routes were reacted with CaH_2 as described above. Figure 3 (top) shows a series of X-ray powder diffraction patterns collected from the products of reaction between the ceramic sample and CaH_2 as a function of reaction time. These data are consistent with the ceramic sample of $SrV_{0.95}Ti_{0.05}O_3$ being a simple mixture of $SrVO_3$ and $SrTiO_3$ which is transformed by the action of CaH_2 into a mixture of $SrVO_2H$ (marked in red) and a small amount of $SrTiO_{3-x}H_x$ (black), precisely as would be expected from previous studies of these perovskite phases in isolation.[12, 26] Synchrotron X-ray powder diffraction data collected from the washed reaction products after 10 days heating confirm these are the reaction products (Figure S2 and Table S3 in the Supporting Information). Thermogravimetric re-oxidation of this sample under flowing oxygen resulted in a 14.5% gain in mass (Figure S3), consistent with the composition detailed in Table S3 (full details of the experiment are described in the Supporting information).

Figure 3 also shows diffraction data collected from the products of reaction between arc-melt prepared $SrV_{0.95}Ti_{0.05}O_3$ and CaH_2. The diffraction pattern taken after 4 days heating looks very similar to the analogous data from the ceramic $SrV_{0.95}Ti_{0.05}O_3$ sample, containing a mixture of CaO, CaH_2, unreacted cubic $SrV_{0.95}Ti_{0.05}O_3$ along with a small amount of a new tetragonal phase which we formulate as '$SrV_{0.95}Ti_{0.05}O_2H$' (red). The *a* lattice parameter of this new phase is very similar to that of undoped

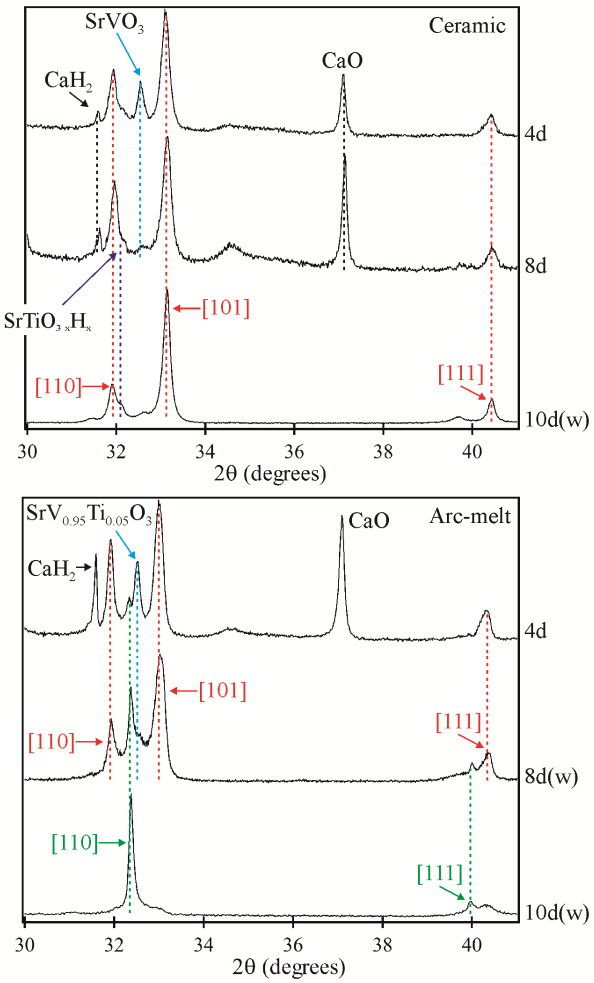

Figure 3. X-ray powder diffraction data collected during the reaction between CaH_2 and $SrV_{0.95}Ti_{0.05}O_3$ prepared by ceramic (top) and arc-melt (bottom) routes. Red symbols indicate positions and Miller indices of tetragonal 'Sr(V/Ti)O_2H' phases, green symbols indicate positions and Miller indices of cubic $Sr(V/Ti)O_{1.5}H_{1.5}$. Data sets marked with a (w) have been washed to remove CaH_2 and CaO.

$SrVO_2H$ (3.929(1) Å vs 3.92331(3) Å), but a distinct elongation along *c*, the V-H-V axis, is apparent (3.738(4) Å vs 3.6671(3) Å). After 8 days of heating, the peaks due to the tetragonal phase reduce in intensity and are replaced by a new cubic phase (*a* = 3.888(1) Å) (green) which eventually becomes dominant after 10 days. Synchrotron X-ray powder diffraction data collected from a sample after 10 days of heating, washed to remove CaH_2 and CaO (Figure 4), can be fitted by a 3-phase model consisting of the dominant cubic phase ($SrV_{0.95}Ti_{0.05}O_xH_y$, 84.3(2)%), a tetragonal phase ($SrV_{0.95}Ti_{0.05}O_2H$, 9.7(4)%) and a minor vanadium metal impurity (5.6(4)%) (Table 2). Thermogravimetric re-oxidation of this sample under flowing oxygen resulted in a 17.2% gain in mass (Figure S4), consistent with a composition of $SrV_{0.95}Ti_{0.05}O_{1.5}H_y$ for the majority cubic phase, as described in detail in the Supporting information. Manganometric titrations indicate an average vanadium/titanium oxidation state of +2.12(3) for the sample (Table S4). When the presence of $SrV_{0.95}Ti_{0.05}O_2H$ and vanadium metal are taken into account, this indicates that the average vanadium/titanium oxidation state in $SrV_{0.95}Ti_{0.05}O_xH_y$ is +2.47(4), consistent with a composition for the majority cubic phase of $SrV_{0.95}Ti_{0.05}O_{1.5}H_{1.5}$ and indicating reduction substantially beyond the V^{3+} level.

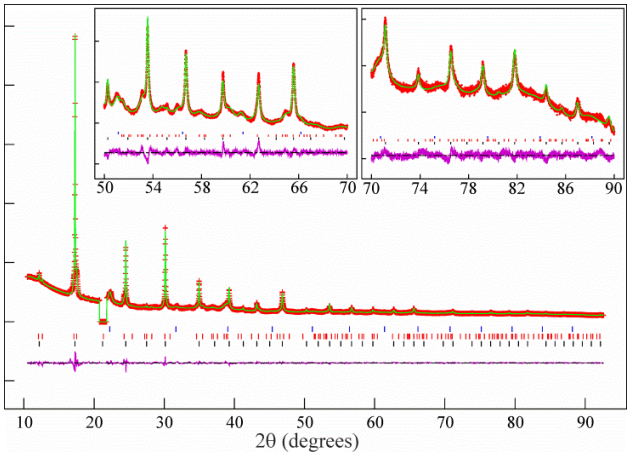

Figure 4. Observed calculated and difference plots from the refinement of $SrV_{0.95}Ti_{0.05}O_{1.5}H_{1.5}$ against synchrotron X-ray powder diffraction data. Lower tick marks indicate peak positions of the majority phase, middle tick marks $SrV_{0.95}Ti_{0.05}O_2H$, upper tick marks elemental vanadium. The excluded region removes a contribution from the 'amorphous' boron used to dilute the sample.

$SrV_{0.95}Ti_{0.05}O_{1.5}H_{1.5}$					
Atom	*x*	*y*	*z*	Fraction	U_{iso} (Å^2)
Sr	½	½	½	1	0.0038(2)
V/Ti	0	0	0	0.95/0.05	0.0024(1)
O/H	½	0	0	0.5/0.5	0.0017(2)
$SrV_{0.95}Ti_{0.05}O_{1.5}H_{1.5}$: space group *Pm*-3*m* (#221) Formula weight : 163.90 g mol^{-1}, Z = 1 Mass Fraction: 84.3(2) % *a* = 3.888(1) Å					
$SrV_{0.95}Ti_{0.05}O_2H$					
Atom	*x*	*y*	*z*	Fraction	U_{iso} (Å^2)
Sr	½	½	½	1	0.0042(3)
V/Ti	0	0	0	0.95/0.05	0.0021(2)
O	½	0	0	1	0.0019(3)
H	0	0	½	1	0.002†
$SrV_{0.95}Ti_{0.05}O_2H$: space group *P*4/*mmm* (#123) Formula weight : 170.40 g mol^{-1}, Z = 1 Mass Fraction: 9.7(4) % *a* = 3.929(1) Å, *c* = 3.738(4) Å					
Vanadium					
V: space group *Im*-3*m* (#229) Formula weight : 50.94 g mol^{-1}, Z = 2 Mass Fraction: 5.6(4) % *a* = 3.032(3) Å					
Radiation source: Synchrotron X-ray, λ = 0.82626(1) Temperature: 298 K χ^2 = 9.625; *wRp*= 3.43 %; *Rp* = 2.31 %.					

Table 2. Structural details from the 3-phase refinement of $SrV_{0.95}Ti_{0.05}O_{1.5}H_{1.5}$ against synchrotron X-ray powder diffraction data. †Thermal parameter of hydride is set at 0.002 Å^2.

Physical characterization of $SrV_{0.95}Ti_{0.05}O_{1.5}H_{1.5}$. Zero-field cooled and field cooled magnetization data collected from $SrV_{0.95}Ti_{0.05}O_{1.5}H_{1.5}$ in an applied field of 100 Oe (Figure 5) can be fitted to the Curie-Weiss law ($\chi = C/(T-\theta) + K$) to yield values of $C = 1.99(3) \times 10^{-2}$ cm^3 K mol^{-1}, $\theta = 2.27(7)$ K, $K = 8.5(1) \times 10^{-4}$ cm^3 K mol^{-1}. The parameters indicate that the majority of the observed magnetization is temperature independent, with the value of the Curie constant corresponding to 0.2% of that expected for S = 1, V^{3+} centers. μ^+SR data collected from $SrV_{0.95}Ti_{0.05}O_{1.5}H_{1.5}$ (Figure S5) show only a relaxation of the polarization and no precession signal that would be associated with long range magnetic order (data collected from the reduced ceramic sample do show oscillations which are due to the presence of magnetically ordered $SrVO_2H$, as expected from previous studies of this material).[12] This combination of physical data indicates that while no local paramagnetic moment can be observed for the vanadium centers, there is no indication of long range magnetic order in $SrV_{0.95}Ti_{0.05}O_{1.5}H_{1.5}$. Transport measurements performed on cold-pressed powder samples of $SrV_{0.95}Ti_{0.05}O_{1.5}H_{1.5}$ indicate that it is insulating.

Discussion

$SrVO_3$-$SrTiO_3$ solubility. The lack of solubility between $SrVO_3$ and $SrTiO_3$ under 'ceramic' conditions is surprising in light of previous reports in the literature describing the complete $SrV_{1-x}Ti_xO_3$ solid solution, studied both as powder and single crystal samples.[27-28] In the former study, powder samples were prepared at higher temperatures than employed under our 'ceramic' conditions (1500 °C, 10% H_2 in argon). However, when we attempted to replicate these high temperature conditions the samples prepared contained large quantities of $SrV_{10}O_{15}$, presumably due to Sr volatility, and so were unsuitable for topochemical reduction studies. In the arc-melting route used here, high temperatures (T > 2000 °C) are applied only for a brief time, and as a result reagent volatility is less of a problem. The increased $SrVO_3$-$SrTiO_3$ solubility observed in samples prepared by arc-melting, in combination with the previous high-temperature synthesis reports, suggests that the $SrV_{1-x}Ti_xO_3$ solid solution is only stable at high temperature, but can be partially quenched as a metastable phase by rapid cooling. This low-temperature meta-stability is confirmed by the observation that when annealed at 1100 °C, 'quenched' $SrV_{1-x}Ti_xO_3$ samples completely separate into simple mixtures of $SrVO_3$ and $SrTiO_3$. As noted above, the arc-melted $SrV_{1-x}Ti_xO_3$ solid solutions still exhibit a degree of phase separation. We attribute the multiphase nature of the arc-melted samples to the limited cooling rate which can be achieved in the arc furnace, which allows for a degree of phase separation on cooling. Despite this partial phase separation, it is clear that in the arc-melted $SrV_{0.95}Ti_{0.05}O_3$ sample, the majority cubic '$SrVO_3$' phase contains some dissolved titanium. Furthermore, annealing studies show that the $SrV_{0.95}Ti_{0.05}O_3$ solid solution is kinetically stable at 600 °C, so the topochemical reduction/anion exchange of $SrV_{1-x}Ti_xO_3$ phases can be studied.

Influence of doping on reaction products. The change in reactivity between $SrVO_3$ and CaH_2 on titanium doping is striking. Unsubstituted $SrVO_3$ reacts readily with CaH_2 to yield $SrVO_2H$, but attempts to advance this reaction further by raising the reaction temperature lead to non-topochemical reactions and, ultimately, to the formation of SrO and metallic vanadium. In contrast, the reaction between CaH_2 and the arc-melted sample of nominal composition $SrV_{0.95}Ti_{0.05}O_3$ proceeds all the way to cubic $SrV_{0.95}Ti_{0.05}O_{1.5}H_{1.5}$, with the direct analogue of $SrVO_2H$, tetragonal '$SrV_{0.95}Ti_{0.05}O_2H$', appearing only transiently as an intermediate phase. These very different reaction outcomes suggest that the presence of even small amounts of titanium dopant destabilizes $SrV_{0.95}Ti_{0.05}O_2H$ in some way, allowing it to react further. Whilst the different reactivity patterns have frustrated our initial goal of

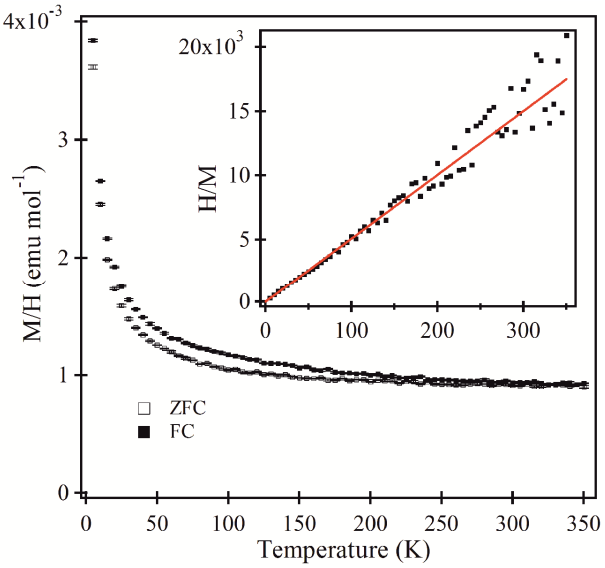

Figure 5. Zero-field cooled and field cooled magnetization data collected from $SrV_{0.95}Ti_{0.05}O_{1.5}H_{1.5}$ in an applied field of 100 Oe. Inset shows approximate fit to the Curie-Weiss law after a large temperature-independent term has been removed.

forming stable hole-doped analogues of $SrVO_2H$, they raise some important questions about the origin of stability in these mixed anion lattices. The lattice parameters of the '$SrV_{0.95}Ti_{0.05}O_2H$' intermediate phase offer some clues to the origin of its relative instability. We noted above that whilst the lattice parameter *a* is marginally shorter than that in unsubstituted $SrVO_2H$ (3.929(1) Å *vs* 3.9331(4) Å), *c* is significantly elongated (3.738(4) Å *vs* 3.6671(3) Å).[12] These changes are consistent with a degree of anion disorder in the Ti-containing phase, with small concentrations of oxide ions along *c* and hydride ions in the *ab* plane causing elongation and contraction, respectively. We note in this context that $SrCrO_2H$ adopts a cubic, anion-disordered structure quite different from that of $SrVO_2H$,[29] suggesting that the anion-ordered tetragonal phase is uniquely stable for a d^2 electronic configuration: deviations to either lower ($SrV_{0.95}Ti_{0.05}O_2H$, $d^{1.95}$) or higher ($SrCrO_2H$, d^3) electron counts appear to drive the system into alternative anion-disordered phases. The partial disordering of the anion lattice adds a large degree of strain to the framework because V-O-V connections are inserted into a lattice optimized for V-H-V links, and *vice versa*, which significantly destabilizes $SrV_{0.95}Ti_{0.05}O_2H$ with respect to anion-ordered $SrVO_2H$.

These observations are supported by a series of DFT calculations performed on the $\sqrt{2} \times \sqrt{2} \times 2$ expanded unit cells shown in Figure 6, each of which contains four transition metal centers. We have studied the two limiting stoichiometries, $SrVO_2H$ and $SrTiO_2H$, as well as $SrV_{0.75}Ti_{0.25}O_2H$, the closest model to the $SrV_{0.95}Ti_{0.05}O_2H$ phase that is accessible within a unit cell of these dimensions. In the *trans* unit cell, the anions are arranged in the same ordered array found in native $SrVO_2H$: *i.e.* with the two hydrides aligned mutually *trans* along the *c* direction. In the *cis* isomer, the hydrides are moved into the *ab* plane and, in the arrangement shown in Figure 6, they are eclipsed in successive *ab* planes. The alternative where the hydrides are staggered in successive planes is computed to be higher in energy in all cases, and is not considered further here. We acknowledge that the *cis* arrangement represents only one possible arrangement amongst the many that could contribute to the anion-disordered cubic phase, but nevertheless a comparison of the two unit cells allows us to assess the energetic cost of moving the hydrides around the lattice. In the case of $SrVO_2H$, the *trans* arrangement of hydride

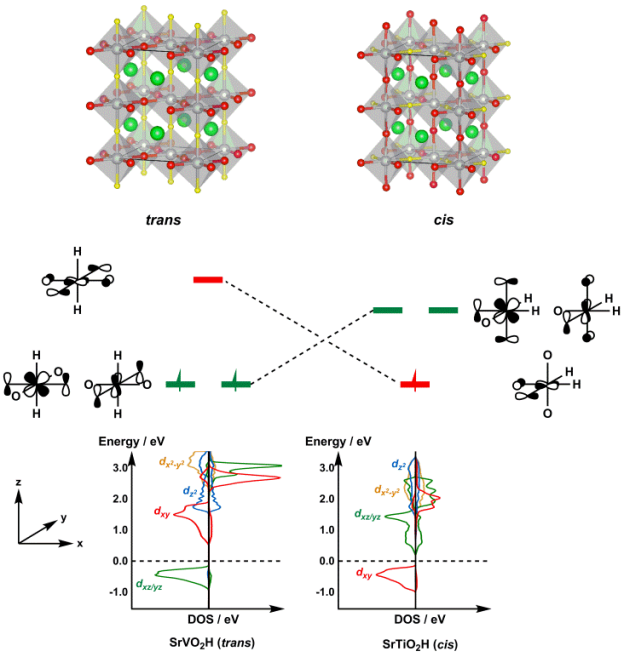

Figure 6. (top) *Trans* and *cis* unit cells used in the computational study. Sr, V, O and H are in dictated by green, grey, red and yellow spheres respectively. (bottom) The calculated density of states for *trans*-$SrVO_2H$ and *cis*-$SrTiO_2H$.

ligands proves to be substantially more stable than the *cis* alternative (ΔE = +0.26 eV per formula unit), consistent with its established preference for the tetragonal phase. In $SrTiO_2H$, in contrast, the order is reversed, with a strong preference for the *cis* arrangement over *trans* (ΔE = -0.21 eV). The mixed metal system $SrV_{0.75}Ti_{0.25}O_2H$ is intermediate between these two limits, with the *trans* structure being favored, but to a much lesser degree than in the all-vanadium analogue (ΔE = +0.09 eV). The calculations therefore indicate that the *trans* arrangement is optimal for the d^2 configuration of V^{3+}, and is progressively destabilized relative to its *cis* analogue as the concentration of Ti^{3+} is increased. We can analyze these differences in terms of two competing factors, the first of which is the strong *trans* influence of the hydride ligand which will in general disfavor mutually *trans* arrangements of hydride ligands. This effect is mediated by the σ framework, and stems from the fact that only a single metal d orbital can participate in both metal-hydride σ bonds when the ligands are *trans* to each other. Superimposed upon this are striking differences in the π character of the two ligands: a hydride is a pure σ donor while an oxide is also a strong π donor, and there is a strong driving force to accumulate oxide ligands in the same plane as vacant metal-based orbitals with dπ character. In the case of $SrVO_2H$, with a d^2 configuration at the metal, these two competing factors are diametrically opposed: the presence of a single vacant dπ orbital (d_{xy}) means that the O-V π bonding is optimal in the tetragonal phase, where all four oxides are aligned in a single plane, but this necessarily forces the two hydrides into a mutually *trans* arrangement. The observed preference for the tetragonal phase indicates that in this case the enhanced π donation from the oxides is the dominant factor. For a d^1 configuration, in contrast, the presence of two vacant dπ orbitals allows for effective O-Ti π bonding in either *cis* or *trans* arrangements, and the σ effects (the *trans* influence) then dominate, imposing a preference for the *cis* arrangement of hydrides. In the $SrV_{0.75}Ti_{0.25}O_2H$ system the arrangement of anions necessarily represents a compromise because it is not possible to simultaneously satisfy the geometric

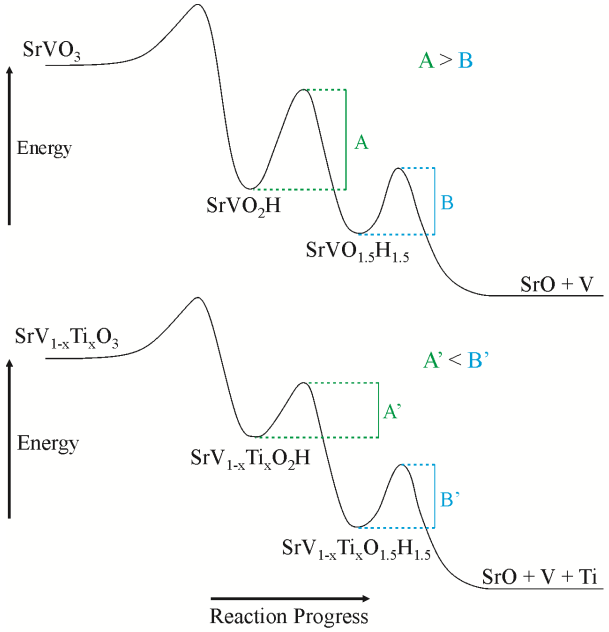

Figure 7. Schematic diagram showing the difference in activation energies for the reduction of $SrVO_3$ and $SrV_{1-x}Ti_xO_3$.

preferences of V (*trans*) and Ti (*cis*) in a single lattice.

The tendency of increasing quantities of Ti in the lattice to reduce the stability of the tetragonal phase suggests that the presence of a stable, anion-ordered tetragonal phase is uniquely associated with a d^2 configuration. Moreover, the properties of the $SrV_{0.95}Ti_{0.05}O_2H$ phase indicate that even a relatively small depletion of the electron density in the dπ band is sufficient to tip the balance in favor of anion disorder. This provides a framework for understanding the different paths followed by the topochemical reactions of CaH_2 with $SrVO_3$ and $SrV_{1-x}Ti_xO_3$. Figure 7 shows schematic reaction-energy profiles for the two cases, where the key difference is that the tetragonal $SrVO_2H$ phase lies in a deeper well on the potential energy surface than the corresponding tetragonal phase for $SrV_{1-x}Ti_xO_2H$. This in turn raises the activation energy for the topochemical reaction that converts $SrVO_2H$ into $SrVO_{1.5}H_{1.5}$, allowing the former to be trapped as a stable species while $SrV_{1-x}Ti_xO_2H$ is only a transiently stable intermediate. Indeed, the absence of detectable amounts of $SrVO_{1.5}H_{1.5}$ indicates that the activation energy for the formation of this compound from $SrVO_2H$ is greater than that for its subsequent decomposition to SrO and metallic V. Even small amounts of titanium substitution significantly degrade the special stability of $SrVO_2H$, making the system more reactive and leading to the observed changes in reaction outcome.

Attempts to dope other phases prepared *via* topochemical reactions have revealed similar but less dramatic responses to cation substitution. For example, attempts to electron dope the Fe^{2+} phase $SrFeO_2$ *via* rare earth substitution for strontium reveal that $RE_xSr_{1-x}FeO_{3-\delta}$ is reduced to $RE_xSr_{1-x}FeO_{2+x/2}$, maintaining an oxidation state of Fe^{2+} in the reduced phase.[30] However, it should also be noted that the sensitivity to cation substitution observed for $SrVO_2H$ and $SrFeO_2$ is not universal in topochemical reduction reactions. For example the conversion of $La_{1-x}A_xMnO_3$ (A = Ba, Sr, Ca) perovskites to $La_{1-x}A_xMnO_{2.5}$ brownmillerite phases containing mixtures of $Mn^{2+/3+}$, is tolerant of a range of A-site compositions and can be readily achieved for $0.15 < x < 0.5$ for A = Sr and $0.22 < x < 0.5$ for A = Ca.[31]

Conclusions

Topochemical reduction of $SrVO_3$ yields the anion-ordered, tetragonal phase $SrVO_2H$. However the analogous reaction conditions applied to hole-doped $SrV_{0.95}Ti_{0.05}O_3$ yields cubic $SrV_{0.95}Ti_{0.05}O_{1.5}H_{1.5}$ not tetragonal $SrV_{0.95}Ti_{0.05}O_2H$. This product, $SrV_{0.95}Ti_{0.05}O_{1.5}H_{1.5}$ is an insulating mixed valent $V^{2+/3+}$ phase, suggesting that the O^{2-}/H^- disorder acts to localize the vanadium d-electrons. Magnetization and μ^+SR data show respectively that the vanadium centers exhibit no local magnetic moment and that there is no indication of (antiferro)magnetic order. This unusual combination of transport and magnetic properties leads us to suggest the system may adopt a network of V-V bonds, although further characterization will be required to rigorously demonstrate this.

Whilst the hole doping of $SrVO_3$ did not, ultimately, achieve the initially intended outcome of producing hole-doped analogues of $SrVO_2H$, the dramatic differences in reactivity in response to seemingly minor changes in composition have encouraged us to consider the factors that determine the outcome of reactions in the solid state. Under typical high-temperature synthetic conditions the products of a reaction are determined by thermodynamic stability and small compositional changes tend not to change the thermodynamic parameters to the extent that some other competing phase becomes more stable. As a result it is generally possible to make small compositional changes to solid phases to tune their physical and chemical behaviour – that is to say these phases are generally 'dopable'. In contrast the products of low-temperature topochemical reactions are selected under kinetic control – the product phase is the one which forms fastest, and is not necessarily the most thermodynamically stable. As a result the products of such reactions depend sensitively on the microscopic mechanism followed by a reaction. The change in reaction product from $SrVO_2H$ to $SrV_{1-x}Ti_xO_{1.5}H_{1.5}$ upon substituting ~5% of the vandium in $SrVO_3$ for titanium shows that even small changes in composition can dramatically alter the relative rates of the competing pathways which exist under low-temperature conditions. Given that this observed sensitivity of the reaction mechansim to chemical compostion is likely to be a general feature of topochemical reactions, we must conclude that a large number of the metastable phases prepared *via* topochemical reactions will, ultimately, prove not to be dopable.

ASSOCIATED CONTENT

Supporting Information

X-ray powder diffraction data from $SrV_{0.5}Ti_{0.5}O_3$ samples. Structural, compositional and μ^+SR characterization of 'reduced' ceramic $SrV_{0.95}Ti_{0.05}O_3$ and $SrV_{0.95}Ti_{0.05}O_{1.5}H_{1.5}$. Details of DFT calculations.

AUTHOR INFORMATION

Corresponding Author

michael.hayward@chem.ox.ac.uk

Author Contributions

The manuscript was written through contributions of all authors. The authors declare no competing financial interests.

ACKNOWLEDGMENT

MAP thanks CONACYT and the Balliol College, Oxford for a scholarship. Experiments at the Diamond Light Source were performed as part of the Block Allocation Group award "Oxford Solid State Chemistry BAG to probe composition-structure-property relationships in solids" (EE13284). Part of this work was carried out at the Swiss Muon Source (SμS), Paul Scherrer Institut, Villigen, Switzerland

REFERENCES

1. Hayward, M. A., Soft chemistry synthesis of oxides. In *Comprehensive Inorganic Chemistry II*, Reedijk, J.; Poeppelmeier, K. R., Eds. Elsevier: Oxford, 2013; Vol. 2, pp 417-453.
2. Schaak, R. E.; Mallouk, T. E., Perovskites by design: A toolbox of solid-state reactions. *Chem. Mater.* **2002,** *14*, 1455-1471.
3. Gopalakrishnan, J., Chimie douce approaches to the synthesis of metastable oxide materials. *Chem. Mater.* **1995,** *7*, 1265-1275.
4. Yamamoto, T.; Kageyama, H., Hydride reduction of transition metal oxides. *Chem. Lett.* **2013,** *42*, 946.
5. Tsujimoto, Y.; Tassel, C.; Hayashi, N.; Watanabe, T.; Kageyama, H.; Yoshimura, K.; Takano, M.; Ceretti, M.; Ritter, C.; Paulus, W., Infinite-layer iron oxide with a square-plannar coordination. *Nature* **2007,** *450*, 1062-1065.
6. Seddon, J.; Suard, E.; Hayward, M., Topotactic reduction of $YBaCo_2O_5$ and $LaBaCo_2O_5$: square-planar Co(I) in an extended oxide. *J. Am. Chem. Soc.* **2010,** *132*, 2802-2810.
7. Hayward, M. A.; Green, M. A.; Rosseinsky, M. J.; Sloan, J., Sodium hydride as a powerful reducing agent for topotactic oxide deintercalation: synthesis and characterisation of the nickel (I) oxide $LaNiO_2$. *J. Am. Chem. Soc.* **1999,** *121*, 8843-8854.
8. Denis Romero, F.; Burr, S. J.; McGrady, J. E.; Gianolio, D.; Cibin, G.; Hayward, M. A., $SrFe_{0.5}Ru_{0.5}O_2$: sqaure-planar Ru^{2+} in an extended oxide. *J. Am. Chem. Soc.* **2013,** *135*, 1838-1844.
9. Hayward, M. A.; Cussen, E. J.; Claridge, J. B.; Bieringer, M.; Rosseinsky, M. J.; Kiely, C. J.; Blundell, S. J.; Marshall, I. M.; Pratt, F. L., The hydride anion in an extended transition metal oxide array - $LaSrCoO_3H$. *Science* **2002,** *295*, 1882.
10. Helps, R.; Rees, N.; Hayward, M., $Sr_3Co_2O_{4.33}H_{0.84}$: An extended transition metal oxide-hydride. *Inorg. Chem.* **2010,** *49*, 11062-11068.
11. Kobayashi, Y.; Hernandez, O. J.; Sakaguchi, T.; Yajima, T.; Roisnel, T.; Tsujimoto, Y.; Morita, M.; Noda, Y.; Mogami, Y.; Kitada, A.; Ohkura, M.; Hosokawa, S.; Li, Z. F.; Hayashi, K.; Kusano, Y.; Kim, J. E.; Tsuji, N.; Fujiwara, A.; Matsushita, Y.; Yoshimura, K.; Takegoshi, K.; Inoue, M.; Takano, M.; Kageyama, H., An oxyhydride of $BaTiO_3$ exhibiting hydride exchange and electronic conductivity. *Nat. Mater.* **2012,** *11*, 507-511.
12. Denis Romero, F.; Leach, A.; Moller, J. S.; Foronda, F.; Blundell, S.; Hayward, M. A., Strontium vanadium oxide-hydrides: 'square-planar' two-electron phases. *Angew. Chem., Int. Ed.* **2014,** *53*, 7556-7559.
13. Goodenough, J. B., *Localized to itinerant electronic transition in perovskite oxides*. Springer-Verlag: Berlin, 2001.
14. Bednorz, J. G.; Muller, K. A., Possible high-Tc superconductivity in the Ba-La-Cu-O system. *Z. Phys. B* **1986,** *64*, 189-193.
15. MacChesney, J. B.; Williams, H. J.; Potter, J. F.; Sherwood, R. C., Magnetic study of manganate phases - $CaMnO_3$ $Ca4Mn_3O_{10}$ $Ca_3Mn_2O_7$ Ca_2MnO_4. *Phys. Rev.* **1967,** *164*, 779-&.
16. Matsumot.G, Study of $(La_{1-x}Ca_x)MnO_{3.1}$ magnetic strucutre of $LaMnO_3$. *J. Phys. Soc. Jpn.* **1970,** *29*, 606-&.
17. Schiffer, P.; Ramirez, A. P.; Bao, W.; Cheong, S. W., Low-temperature magnetoresistance and the magnetic phase-diagram of $La_{1-x}Ca_xMnO_3$. *Phys. Rev. Lett.* **1995,** *75*, 3336-3339.
18. Liu, K.; Hou, Y. S.; Gong, X. G.; Xiang, H. J., Orbital delocalization and enhancement of magnetic interactions in perovskite oxyhydrides. *Scientific Reports* **2016,** *6*.
19. Wei, Y. F.; Gui, H.; Li, X.; Zhao, Z. J.; Zhao, Y. H.; Xie, W. H., The effect of hydrogen ordering on the electronic and magnetic properties of the strontium vanadium oxyhydride. *J. Phys.:Condens. Matter* **2015,** *27*.
20. Yamamoto, T.; Zeng, D.; Kawakami, T.; Arcisauskaite, V.; Yata, K.; Patino, M. A.; Izumo, N.; McGrady, J. E.; Kageyama, H.; Hayward, M. A., The role of π-blocking hydride ligands in a pressure-induced insulator-to-metal phase transition in $SrVO_2H$. *Nature Communications* **2017,** *8*, 1217.
21. Rey, M. J.; Dehaudt, P.; Joubert, J. C.; Lambertandron, B.; Cyrot, M.; Cyrotlackmann, F., Preparation and structure of the compounds $SrVO_3$ and Sr_2VO_4. *J. Solid State Chem.* **1990,** *86*, 101-108.
22. Larson, A. C.; Von Dreele, R. B. *General Structure Analysis System*, Los Alamos National Laboratory Report LAUR 86-748: 2000.

23. Kresse, G.; Furthmuller, J., Efficient iterative schemes for ab initio total-energy calculations using a plane-wave basis set. *Phys. Rev. B* **1996,** *54*, 11169-11186.

24. Perdew, J. P.; Burke, K.; Wang, Y., Generalized gradient approximation for the exchange-correlation hole of a many-electron system. *Phys. Rev. B* **1996,** *54*, 16533-16539.

25. Schmidbauer, M.; Kwasniewski, A.; Schwarzkopf, J., High-precision absolute lattice parameter determination of $SrTiO_3$, $DyScO_3$ and $NdGaO_3$ single crystals. *Acta Crystallographica Section B-Structural Science Crystal Engineering and Materials* **2012,** *68*, 8-14.

26. Sakaguchi, T.; Kobayashi, Y.; Yajima, T.; Ohkura, M.; Tassel, C.; Takeiri, F.; Mitsuoka, S.; Ohkubo, H.; Yamamoto, T.; Kim, J. E.; Tsuji, N.; Fujihara, A.; Matsushita, Y.; Hester, J.; Avdeev, M.; Ohoyama, K.; Kageyama, H., Oxyhydrides of (Ca,Sr,Ba)TiO_3 perovskite solid solutions. *Inorg. Chem.* **2012,** *51*, 11371-11376.

27. Hong, K. Y.; Kim, S. H.; Heo, Y. J.; Kwon, Y. U., Metal-insulator transitions of $SrTi_{1-x}V_xO3$ solid solution system. *Solid State Comm.* **2002,** *123*, 305-310.

28. Tsuiki, H.; Kitazawa, K.; Fueki, K., The donor level of V^{4+} and the metal-nonmetal transtion in $SrTi_{1-x}V_xO_3$. *Japanese Journal of Applied Physics Part 1-Regular Papers Brief Communications & Review Papers* **1983,** *22*, 590-596.

29. Tassel, C.; Goto, Y.; Kuno, Y.; Hester, J.; Green, M.; Kobayashi, Y.; Kageyama, H., Direct synthesis of chromium perovskite oxyhydride with a high magnetic-transition temperature. *Angew. Chem., Int. Ed.* **2014,** *53*, 10377-10380.

30. Yamamoto, T.; Ohkubo, H.; Tassel, C.; Hayashi, N.; Kawasaki, S.; Okada, T.; Yagi, T.; Hester, J.; Avdeev, M.; Kobayashi, Y.; Kageyama, H., Impact of lanthanoid substitution on the structural and physical properties of an infinite-layer iron oxide. *Inorg. Chem.* **2016,** *55*, 12093-12099.

31. Parsons, T. G.; D'Hondt, H.; Hadermann, J.; Hayward, M. A., The synthesis and structural characterisation of of $La_{1-x}A_xMnO_{2.5}$ (A = Ba, Sr, Ca) phases – mapping the variants of the brownmillerite structure. . *Chem. Mater.* **2009,** *21*, 5527.

For Table of Contents Only. Titanium substitution dramatically changes the outcome of the anion exchange of $SrVO_3$, yielding $SrV_{1-x}TiO_{1.5}H_{1.5}$, not $SrV_{1-x}TiO_2H$. This dramatic change in reactivity is attributed to an electronic destabilization of $SrVO_2H$ on titanium substitution. DFT calculations indicate that the presence of an anion-ordered, tetragonal $SrMO_2H$ phase is uniquely associated with a d^2 electron count, and that titanium substitution leads to an electronic destabilization of $SrV_{1-x}Ti_xO_2H$ phases which, ultimately, drives further reaction of $SrV_{1-x}Ti_xO_2H$ to $SrV_{1-x}Ti_xO_{1.5}H_{1.5}$.